DSC-Vol. 42, Advances in Robotics
ASME 1992

DESIGN AND IMPLEMENTATION OF A FORCE REFLECTING MANIPULANDUM FOR MANUAL CONTROL RESEARCH

Bernard D. Adelstein
Aerospace Human Factors Research Division
NASA-Ames Research Center
Sterling Software
Moffett Field, California

Michael J. Rosen
Department of Mechanical Engineering
Massachusetts Institute of Technology
Cambridge, Massachusetts

ABSTRACT

This paper describes a force reflecting interface developed to apply programmable mechanical loads to the human arm for the experimental study of a specific component of manual output: tremor. Because it was designed to meet the performance requirements for effective dynamic coupling with tremor, the interface is also capable of producing high bandwidth simulations of general mechanical environments for interaction with volitional human movement.

The interface is a two degree of freedom manipulandum (*i.e.*, backdriveable manipulator) based on a novel spherical 5R closed chain linkage that joins the output of two DC motors to a handle grasped by the human subject/operator. This linkage configuration provides high structural bandwidth and permits approximate Cartesian control of endpoint impedances without geometric computation. The computational burden for real time control of manipulandum load simulations is further reduced by a hardwired digitally supervised analog controller that makes use of directly sensed displacements, velocities, and accelerations at the two motor shafts and forces at the human-machine interface.

INTRODUCTION

The goal of this work was the development of a research apparatus for applying controlled mechanical loads to the human arm for the study of a particular component of human manual output: tremor. The device constructed to fulfill the performance requirements for this research has the general form of a backdriveable powered manipulator—a design common to force reflecting manual interfaces for both virtual environment and teleoperation applications. While the quantitative performance specifications for this device were dictated primarily by the characteristics of human tremor, many of the design issues considered here are pertinent to the development of effective kinesthetic coupling for force reflecting manual interfaces in general.

Thus, in this paper, we motivate the design of our force reflecting interface with a brief review of the characteristics, causes, and consequences of tremor in human movement. Based on the characteristics of human tremor, we develop quantitative performance goals for the design of our apparatus. Details of our design follow. Included are the device's theoretical kinematics, hardware implementation, and a simple structural bandwidth model. An overview of the system's load control architecture and safety procedures completes the description of the device.

MOTIVATION

Tremors are involuntary oscillations that are superimposed on the volitional neuromuscular output of all body parts, in both able bodied and neurologically impaired individuals. Normal tremor in healthy people is small in amplitude and typically requires special instrumentation to demonstrate its presence. Pathological tremors are visually obvious and can be severe enough to obscure concomitant voluntary muscular activity to the point of functional impairment. Oscillatory frequency content can range from as low as 1.5 Hz in certain pathological conditions up to 12 Hz for normal tremor.

Thorough knowledge of the causes of various normal and pathological tremor types is vital for the accurate diagnosis of related neurological disorders, and for the effective prescription of pharmacological, surgical, and rehabilitation treatments. Since tremor signals are propagated along the same physiological "hardware" as volitional movement, understanding the mechanisms governing tremor generation may also offer insight into the planning and organization of volitional neuromuscular activity.

Experimental, clinical, and analytic research have led to the proposal of a number of tremogenic (*i.e.*, tremor generating) mechanism hypotheses.[1] The hypothesized

[1] See Desmedt (1978) and Findley and Capildeo (1984) for a review.

mechanisms fall into three broad categories: 1) autonomous pacemakers in the brain and spinal areas; 2) tuned resonance of limb biomechanics; and 3) marginal stability due to conduction latencies in neuromuscular reflex loop pathways.

Controlled mechanical loading has served as a useful noninvasive probe for the experimental identification of tremogenic mechanisms. For example, systematic changes in oscillatory tremor frequency occurring with externally augmented limb inertia or joint stiffness have implicated biomechanical resonance as a factor in certain tremor types (Stiles and Randall, 1967). The role of reflex loop latency has been inferred from the ability of pulsed mechanical perturbations to re-entrain the steady state phase of tremor oscillations (Lee and Stein, 1981). Absence of tremor response to externally applied mechanical loads has suggested that some tremors are caused by autonomous pacemakers.

To date, tremogenic mechanism studies have only involved carefully constrained *single* kinematic degree of freedom (*i.e.*, single joint) mechanical loading experiments.[2] Pathological and normal *whole limb* tremors present during less restricted activities of daily living (ADL) have not yet been subjected to the same systematic examination of mechanical load response. In addition to the identification of tremogenic mechanisms for whole limb oscillations, controlled mechanical loading experiments in more than one degree of freedom would allow issues of neural, muscular, and mechanical coupling between tremors in different degrees of freedom to be examined. Ultimately, normal and pathological tremor models based on data from multisegment limb loading experiments are key to objective functional assessment, the effective prescription of treatment regimens, and the efficient design of practical assistive devices for tremor disability.

PERFORMANCE REQUIREMENTS

The fundamental requirements for our tremor loading interface are as follows. The interface must enable loads to be imposed at the human arm. The loads should be accurately controllable in real-time, based on concurrent measurements of kinematics and forces. The loading should be versatile—*i.e.*, programmable to emulate a broad range of passive and active mechanical loads.

We chose the arm as the human interaction port for our device because of the significance of manual control as part of normal ADL and the corresponding need to understand how pathological tremors may corrupt this important function. In this section, the performance requirements for versatile real-time load control necessary for dynamic interaction with whole-arm tremor are specified. How these specifications pertain to dynamic interaction with normal volitional arm activity is also discussed.

Dynamic Range

The goal of versatile loading implies that the interface is capable of applying a broad variety of mechanical loads within a fixed performance envelope. For the practical purposes of a tremor research interface (or any general kinesthetic interface), this envelope means that one need not design for performance beyond the requirements of the application.

Two related methods may be used to define quantitatively the performance envelope required for effective dynamic coupling between the loading interface and a human arm. Since dynamic coupling implies bidirectional mechanical power exchange, one approach would be to consider the range of expected human arm impedances for a particular set of conditions (such as tremor), and design the interface's impedance range accordingly. The second approach, discussed below, is to look directly at the quantities from which impedances can be calculated—*i.e.*, the forces and related kinematics over the bandwidth of a given set of human arm activities.

Matthews and Muir (1980) reported tremors with 10 N maximum peak-to-peak magnitude and 4 N rms magnitude in the 6 to 12 Hz band, at the forearm of healthy subjects as a consequence of 160 N of voluntary elbow flexion forces. Albers, Potvin, Tourtellotte, Pew, and Stribley (1973) noted 2 N peak-to-peak maximums for 5 to 11 Hz oscillations at the hand due to unconstrained *parkinsonian* arm tremor. Riley and Rosen (1987), in unpublished data, measured larger oscillatory force levels up to 40 N peak-to-peak between 2 and 5 Hz in subjects with severe pathological whole arm *intention* tremors.

By comparison, the *volitional* force output of upper percentile adult males can surpass 1000 N at the hand, depending on arm posture, when pressing on an isometric (*i.e.*, rigid) interface (Van Cott and Kinkade, 1972). "Torque-speed" curves representing maximal and normal levels of elbow activity in average adult males show that these large forces trail away rapidly as arm speed is increased (Livingstone and Crecraft, 1968).

Tremor is of additional interest here because its frequency confers an upper bound on the fundamental frequency of repetitive alternating limb movement or force that can be achieved voluntarily (Freund, Hefter, Homberg, and Reiners, 1984). Freund *et al.* (1984) also observed that the full amplitude of volitional human movement and force can only be maintained up to approximately 3 Hz. Stiles (1975) noted that repetitive *volitional* hand motion has significant energy content not only at the fundamental movement frequency, but at its first harmonic (*i.e.*, double the fundamental frequency) as well. Thus, the quantitative performance levels necessary for tremor research can also help define the bandwidth and force requirements to design interfaces that couple effectively with the dynamics of human movement in general.

As a consequence of the prior tremor measurements listed above, a ±20 N (40 N peak-to-peak) sustained force capability over an "effective operating bandwidth" from 0 to 12 Hz was set as a design objective for our arm loading interface. Effective operating bandwidth implies that the interface should be able to produce forces which accurately track human arm activity within these magnitudes and frequencies. To ensure that the interface is able to achieve the desired tracking fidelity, the total phase lag contribution from all hardware components (*i.e.*, actuators, mechanical linkage, sensors, and peripheral electronics) and the load controller itself should be minimized—or, equivalently, their individual bandwidths should be maximized. For instance, maximizing electromechanical actuator bandwidth means selecting components with the fastest electrical and mechanical time constants; for the mechanical linkage, both structural inertia and compliance should be reduced. With respect to

[2] See Adelstein (1989) for a review.

the load controller, data sampling rates should be increased and update latencies reduced by minimizing the amount of computation needed for real-time control.

Threshold and Resolution

Threshold and resolution determine how finely the controlled mechanical load can be regulated within the interface dynamic range envelope described above. The loading threshold corresponds to the minimum effort required of the human operator to overcome static or kinetic friction and move (*i.e.*, accelerate) the interface when the load controller is commanded to produce zero force.

The friction threshold level affects the interface's backdriveability. If friction is too large, the human operator cannot move the interface. Ideally, the human should be able to push on the interface linkage and, as a consequence, backdrive the interface actuators as readily as the actuators can move the human's limb. Based on Bejczy and Salisbury (1980), a static friction level of 5 percent of the full dynamic force range was set as a design goal for this work.

Once above this threshold level, factors related to resolution affect how accurately the controlled load can be transferred through the interface to the human and vice versa. Quantities that can affect load control resolution include the backlash, cogging, and ripple present in different types of actuators and mechanical transmission elements. The effects of threshold and resolution factors can be minimized by selection of appropriate mechanical components and through design of the controller.

Degrees of Freedom

The number of degrees of freedom (dofs) affect the complexity of the loading interface design. The most difficult to design and control would be a linkage with a sufficient number of actuators to individually oppose each of the 37 or so muscles that span the shoulder, elbow, and wrist joints of the human arm. An alternative would be a device such as the ones described by Jacobsen, Smith, Backman, and Iversen (1991) and Jau (1991) which completely accommodate the redundant seven dof kinematics of these three arm joints. A more general solution would be to develop a six dof interface [*e.g.*, Bejczy and Salisbury (1980)] that could match the complete kinematics of any single limb segment.

In this work, we elected to develop a two dof configuration. Such a configuration would offer design and control simplicity in comparison with the six and seven dof devices cited above, and, as a result, reduce design and component costs. It would, however, enable experiments in which tremor load response could be examined in greater than the one degree of freedom of earlier studies and still permit many of the arm motions associated with ADL.

Reference Frame

A second configuration issue is where to locate the reference frame for the forces developed by the loading interface. One alternative is a moving "non-inertial" base attached to another body segment on the experimental subject's arm or torso. This means that the other body segment must sustain the reaction to the interface loading force—e.g., a spring force applied to the arm produces an equal and opposite spring force at the other body part. This choice is unsatisfactory for tremor research because oscillatory tremor forces with pathological amplitude would have to be absorbed by another site on the subject's body.

Our choice for the reference frame is a mechanical ground fixed with respect to the earth. This obviates the experimental subject having to provide the reaction necessary to oppose tremor and load forces. An additional reason for choosing a fixed ground becomes apparent after the discussion below of actuator type and mechanism configuration for the loading interface: the subject does not have to carry the substantial mass of the loading interface hardware.

Range of Motion

A minimum workspace of 15 cm square for human hand motion, over which the full ±20 N dynamic force requirement for tremor loading had to be met, was set as a design goal for the interface. This workspace size was considered sufficient to allow the range motion and dynamics necessary for simulating many common two degree of freedom ADL—*e.g.*, writing or drawing on a piece of paper, stirring a cooking pot, or moving an automobile stick shift.

Based on a worst case assumption of 6 Hz pathological tremor capable of spanning the full 15 cm workspace, peak interface design velocities of 300 cm/sec were estimated.

Safety

The potential for dangerous incidents when a human interacts directly with a powered mechanical device cannot be understated. Thus, a principal design concern for the interface is that it pose no hazard to the experimental subject, both under normal operation and during unexpected fault conditions.

The passive (*i.e.*, unpowered) device must be mechanically safe. It should be free of sharp edges and confining spaces that may cut or pinch, and must not demand awkward or uncomfortable postures of the subject. Under normal active (*i.e.*, powered) conditions, the forces, accelerations, and velocities applied to the human should be restricted, both for transient situations as well as over extended periods of operation. During sudden interface fault conditions, there must be reliable detection of errant behavior and effective, reliable reaction to the problem.

Since, ultimately, the interface's power source will be electrical and its controller electronically based, safeguards against electric shock—including proper insulation, grounding, and fusing procedures—must be implemented.

Portability

Possible sites for use of the loading interface include not only the laboratory at M.I.T., but clinical and home environments as well. Thus, the interface should not have specialized mechanical actuation requirements—*i.e.*, it should not rely on fixed base (or bulky portable) hydraulic or pneumatic pumps, compressors, and reservoirs. Likewise, all electric power needs should be met by conventional 115 volt AC single phase service, without exceeding standard 20 A single circuit capacity.

Type of Actuation

Hydraulic actuation was further precluded for the interface because of the potential of even minor fluid leakage from imperfectly sealed lines to undermine cleanliness and safety when working at other sites in addition to the

laboratory at M.I.T. Pneumatics were abandoned early in the design process since the compressibility and resultant compliance of air at moderate pressures were not considered suitable for this application. Because of these concerns, electromechanical actuation, the remaining commercially available mechanical power source, was selected to provide the loading capability for the interface.

MECHANICAL CONFIGURATION

Implications of Configuration

Having decided on a two dof electromechanically actuated device for the programmable arm loader, our objective was to design a fixed base mechanical linkage that couples the human to powered electric motors, subject to the bandwidth and backdriveability performance constraints listed above. The choice of linkage and motor configuration involves many of the same design considerations that must be addressed for robotic manipulators. In this section we review some conventional manipulator configurations and propose a novel linkage design for our arm loading manipulandum.[3]

The typical industrial electromechanical manipulator has a single degree of freedom actuator associated with each kinematic dof. Relative motion for each dof takes place across a simple revolute (R) or prismatic (P) joint (lower pair), which is in turn separated from other joints in the mechanism by links. Some familiar two dof serial link mechanisms include 2R armlike mechanisms with co-planar joints, 2R spherical mechanisms with orthogonal joints, and 2P Cartesian mechanisms with orthogonal axes.

The actuation for a particular dof is described as "direct drive" if the motor is situated exactly at the joint, with its base (stator) attached to, or part of, the first link and its moving element (rotor) attached to the second link. Manipulators with this type of actuation have been called direct drive robots. The distinct advantage of direct drive is the absence of transmission elements that cause undesirable dynamics, and compromise backdriveability. The cost entailed with direct-drive, however, is that each link must carry the next link's actuator. This means that the link inertia is not only increased by the mass of the actuator, but also by the added material required to stiffen structurally the link supporting the added actuator mass. The result of the increased inertia is lower mechanical bandwidth and reduced acceleration capability.

One alternative to massive manipulators carrying bulky actuators at each joint, is to locate the actuators at the base of the manipulator (*i.e.*, mechanical ground) and drive the links remotely through transmissions made up of higher kinematic pairs. However, as noted above, many of these transmission elements can introduce undesirable dynamics that affect bandwidth and backdriveability. Belts, cables, and flexible drive shafts make for a compliant coupling between actuator and end effector. Gears, lead screws, and chain drives can cause backlash. All of these transmission types can add friction to the device.

A second alternative is to employ closed kinematic chains for the mechanical transmission that are composed of only lower pairs and rigid links. An example of this transmission type is the revolute joint parallelogram mechanism used to transfer torque from an actuator at mechanical ground to the distal "elbow" joint of planar armlike devices (Asada and Youcef-Toumi, 1984). In addition to having less inertia because actuators are not carried, these lower pair "parallel" closed chain configurations offer less friction and greater stiffness than the higher pair transmission elements listed in the previous paragraph. In general, the drawbacks of parallel mechanisms are restricted linkage motion because of the additional link elements required to close the kinematic chain, and tighter fabrication tolerance requirements to prevent assembly misalignments that could cause excessive friction or binding.

The design of the manipulator linkage and transmission not only affects device dynamics, but also plays a major role in system control. For the two dof arm loading manipulandum, our objective is to regulate interface forces and kinematics with respect to a fixed Cartesian reference frame. Unless the device configuration itself is Cartesian (*i.e.*, orthogonal with prismatic pairs), the transformation from joint space quantities to endpoint kinematics and quasi-static forces demands repetitive trigonometric computation. In dynamic cases, the computation issue becomes more involved. In addition to trigonometric transformations, nonlinear velocity terms must be calculated for the compensation of Coriolis and centripetal effects.

One approach to simplifying computation is to design manipulators that are computationally "clean"—clean in the sense that they do not have undesirable dynamic or geometric properties that need to be compensated through computationally intensive control algorithms. Asada and Youcef-Toumi (1984) demonstrated this tactic for simplifying manipulator control through mechanical design by dynamically balancing parallel planar five bar linkages to eliminate Coriolis and centripetal coupling between actuators. It should be noted, however, that their manipulators were only decoupled in joint angle space. Control of force or motion in decoupled orthogonal manipulator endpoint coordinates—except at specific joint angle configurations for a restricted set of link length designs—still required computation of measurement based geometric and kinematic transformations.

Spherical Mechanism Design

In this paper we describe a closed chain configuration that permits *approximate* endpoint decoupling of planar forces and kinematics without geometric computation, based on local control of the actuators in joint angle space. The configuration eliminates the need for one actuator to carry the inertia and weight of the second dof's actuator by fixing both actuator housings to a common mechanical ground. Since the mechanism design is composed of rigid links with revolute lower pairs, transmission friction, backlash, and compliance are minimized.

The inspiration for the design of the force loading interface is the conventional position sensing joystick mechanism illustrated in Figure 1. To use the conventional joystick, the human operator grasps the handle (*G*) and pivots the handle shaft about the spherical joint (*H*). The intersection of the handle shaft with the two slotted

[3] A backdriveable manipulator linkage used for the study of human or animal hand motion is called a manipulandum (*e.g.*, Schmidt, 1973).

swing arm yokes at point J causes swing arm A to rotate about axis #1 (C-D) and swing arm B to rotate about axis #2 (E-F). In some joysticks, a rectangular block at J prevents rotation of the handle shaft about its long axis with respect to one of the slotted yokes. Goniometers (typically electronic rotary potentiometers), coupled to each slotted yoke along axis #1 and #2, sense swing arm angles, thereby allowing the handle shaft's two dof position to be determined.

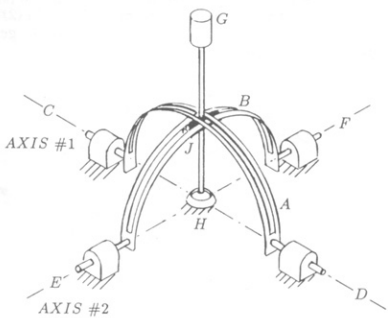

Figure 1. Two dof slotted swing arm joystick mechanism. This is a modified version of the standard commercial joystick configuration. Normally, the swing arms lie below the *CDEF* plane and the handle shaft intersects with the slots beneath the spherical joint *H*.

For a force loading interface, the goal is to replace the goniometers with rotary electric motors so that motor torques move the handle, and forces applied at the handle rotate the motor shafts. The shortcoming of the conventional joystick mechanism, however, is that the travel of the handle shaft through the slots in the swing arms and the rotation of the ball inside the socket of the spherical joint are subject to friction.[4] In the conventional joystick, friction can be reduced by widening the slots and loosening the ball and socket joint. Unfortunately, this also increases backlash, causing uncertainty in the position of the handle shaft relative to the angle measured at the #1 and #2 axes.

The solution to the friction and backlash problem is to replace all kinematic pairs in the joystick mechanism with simple revolute joints. To accomplish this, the essential features of the joystick measurement are first reduced to two revolute joints mounted on a common mechanical ground and a spherical pair at the intersection of the orthogonal and coplanar #1 and #2 axes as shown in Figure 2. The next step is to break down the spherical pair into the equivalent set of three intersecting, non-colinear, single degree of freedom revolute pairs (j_3, j_4, and j_5) depicted in Figure 3. The joystick handle shaft is then simply extended from the link between joints j_4 and j_5. The single dof revolute pairs j_1 and j_2 along axes #1 and #2 remain unaltered. The resultant five link closed chain mechanism (four bars plus mechanical ground) is recognized as being equivalent to the 5R spherical mechanism shown in Figure 4.[5]

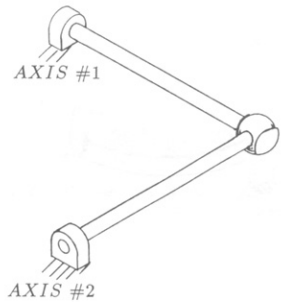

Figure 2. Essential pairs of the standard joystick mechanism.

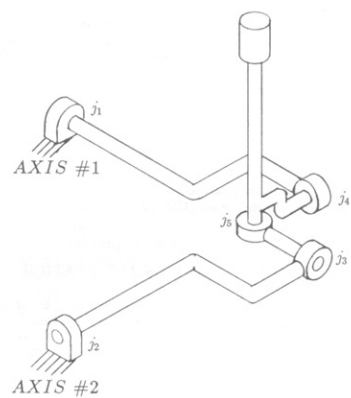

Figure 3. Five link joystick mechanism.

[4] Chaware and Amarnath (1984) proposed the use of a conventional two dof joystick mechanism as part of a robot wrist. They did not attempt to alleviate the device's inherent friction and backlash.

[5] Carmichael (1979) demonstrated the equivalence of the standard joystick mechanism with the spherical 5R closed chain linkage through a different approach.

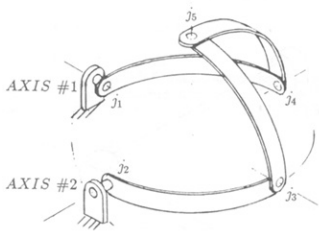

Figure 4. Spherical five bar mechanism.

A mobility analysis of the spherical linkage follows from the Kutzbach/Grübler criterion for planar mechanisms. On a spherical surface, l links each have three degrees of freedom and each of the j revolute joints removes two of those degrees of freedom. Since the position and orientation of the ground link are arbitrary on the surface of the sphere, the mobility, m, is given by

$$m = 3(l - 1) - 2j . \tag{1}$$

Thus, for the closed chain five bar with $l = j = 5$, $m = 2$, verifying that the kinematics of the 5R spherical closed chain mechanism can be fully described by two generalized coordinates—the same as for the conventional swing arm joystick.

MANIPULANDUM KINEMATICS AND STATICS

The two plane model in Figure 5 is constructed to help develop a mathematical description of the 5R closed chain manipulandum. The resulting equations allow torques and rotations at joints j_1 and j_2 to be related to Cartesian forces and displacements at the manipulandum handle.

Geometric Relations

The plane P_1 in Figure 5 can be thought of as replacing the swing arm A in Figure 1, rotating through angle α about axis #1. Similarly, P_2 replaces swing arm B, and rotates through β about axis #2. Together, the two angles α and β are generalized independent variables that completely describe joystick mechanism handle position.

The orientation of the joystick handle link with respect to the fixed (x,y,z) reference frame coincides with $\mathbf{n}_3$, the intersection of the two rotating planes, where

$$\mathbf{n}_3 = \frac{\cos\alpha \sin\beta}{\sqrt{1 - \sin^2\alpha \sin^2\beta}}\mathbf{i} - \frac{\sin\alpha \cos\beta}{\sqrt{1 - \sin^2\alpha \sin^2\beta}}\mathbf{j} + \frac{\cos\alpha \cos\beta}{\sqrt{1 - \sin^2\alpha \sin^2\beta}}\mathbf{k} , \tag{2}$$

is derived from the cross product of the unit surface normals $\mathbf{n}_1$ and $\mathbf{n}_2$. The denominator term in Equation (2) is necessary to scale $\mathbf{n}_3$ into a unit vector because, in general, $\mathbf{n}_1$ and $\mathbf{n}_2$ are generally not orthogonal.

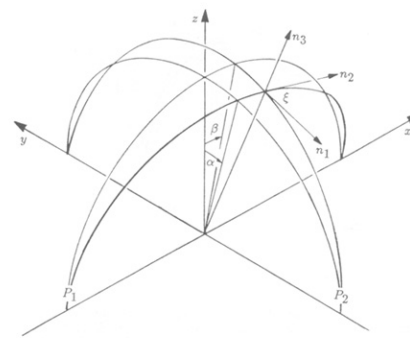

Figure 5. Two plane model joystick construction.

The nonorthogonality between $\mathbf{n}_1$ and $\mathbf{n}_2$ is given by $|\,90° - \xi\,|$, where

$$\xi = \cos^{-1}(\sin\alpha \sin\beta). \tag{3}$$

ξ remains small (less than 10°), indicating that the planes P_1 and P_2 remain nearly perpendicular over the design operating range $|\,\alpha\,|, |\,\beta\,| \le 25°$. In addition, over this range,

$$0.98 < \sqrt{1 - \sin^2\alpha \sin^2\beta} \le 1, \tag{4}$$

allows the denominator term in Equation (2) to be treated for practical purposes as being approximately equal to unity.

Kinematic Description

The kinematic description of the manipulandum is developed from the geometric transformation between natural joystick coordinates and the fixed Cartesian coordinates of Figure 5. However, before proceeding, a third general displacement variable, r, that lies along the handle orientation vector, $\mathbf{n}_3$, is included to make available an (α,β,r) based coordinate description of three dimensional space.

This third coordinate is necessary because the manipulandum angles α and β alone only describe a constant radius two dimensional spherical surface. While there is a two-to-three dimensional mapping from the spherical surface into the global (x,y,z) coordinate frame, the mapping is not invertible because there are an infinity of points that are not on the sphere which cannot be transformed back into the two dimensional (α,β) space.

Thus, by multiplying each Cartesian component of Equation (2) by the variable r, the general three-to-three invertible mapping, $\mathbf{x} = \mathbf{L}(\mathbf{q})$, where $\mathbf{x} = [x\ ,\ y\ ,\ z]^{\mathrm{T}}$ and $\mathbf{q} = [\alpha\ ,\ \beta\ ,\ r]^{\mathrm{T}}$, can be stated fully as

$$x = \frac{r\cos\alpha\sin\beta}{\sqrt{1-\sin^2\alpha\sin^2\beta}} \tag{5}$$

$$y = \frac{-r\sin\alpha\cos\beta}{\sqrt{1-\sin^2\alpha\sin^2\beta}} \tag{6}$$

$$z = \frac{r\cos\alpha\cos\beta}{\sqrt{1-\sin^2\alpha\sin^2\beta}} \tag{7}$$

It is then straightforward to derive the Jacobian,

$$\mathbf{J} = \frac{\partial \mathbf{x}}{\partial \mathbf{q}}\ , \tag{8}$$

to relate infinitesimal displacements, instantaneous velocities, and higher order kinematics between the $\mathbf{x}$ and $\mathbf{q}$ coordinate systems.

Singularities in the manipulandum workspace correspond to the values of α, β, and r at which the Jacobian is not invertible, *i.e.*, where

$$\det \mathbf{J} = \frac{(1-\sin^2\alpha\sin^2\beta\ )^{3/2}}{r^2\cos\alpha\cos\beta} = 0\ . \tag{9}$$

According to l'Hôpital's rule, det $\mathbf{J}$ is zero valued when either α or β equal ± 90 degrees. The α and β singularities do not imply that the handle shaft cannot pass through the x-y plane of Figure 5. They do, however, indicate that it is impossible to use actuator rotations at joints j_1 and j_2 to change the orientation the handle shaft while still keeping the handle constrained to the x-y plane. Note that the mechanism singularities occur well beyond the $|\alpha\ |,\ |\beta\ | \leq 25°$ operating range of the manipulandum.

Static Forces

Static forces at the manipulandum handle, $\mathbf{F}$, can be related to a vector of internal joystick torques and force, $\mathbf{P}$, according to

$$\mathbf{F} = \mathbf{J}^{-\mathrm{T}}\,\mathbf{P} \tag{10}$$

where $\mathbf{F} = [F_x\ ,\ F_y\ ,\ F_z\ ]^{\mathrm{T}}$ is the force component vector at the handle interface in the Cartesian coordinates of Figure 5. $\mathbf{P} = [\tau_\alpha\ ,\ \tau_\beta\ ,\ F_r\ ]^{\mathrm{T}}$ consists of τ_α and τ_β, the torques at the manipulandum actuator shafts, and F_r, the force along the length of the joystick handle.

The transformation of static manipulandum *actuator* torques τ_{m_α} and τ_{m_β} into controlled force components F_{m_x}, F_{m_y}, and F_{m_z} at the joystick handle interface follows directly from Equation (10):

$$F_{m_x} = \left[\frac{\cos\beta\sqrt{1-\sin^2\alpha\sin^2\beta}}{R_o\cos\alpha}\right]\tau_{m_\beta} \tag{11}$$

$$F_{m_y} = -\left[\frac{\cos\alpha\sqrt{1-\sin^2\alpha\sin^2\beta}}{R_o\cos\beta}\right]\tau_{m_\alpha} \tag{12}$$

$$F_{m_z} = -\left[\frac{\sin\alpha\sqrt{1-\sin^2\alpha\sin^2\beta}}{R_o\cos\beta}\right]\tau_{m_\alpha} - \left[\frac{\sin\beta\sqrt{1-\sin^2\alpha\sin^2\beta}}{R_o\cos\alpha}\right]\tau_{m_\beta}\ , \tag{13}$$

where R_o is the constant handle length between the center of the interface handgrip and the center of joystick rotation at the origin of the (x,y,z) coordinate frame.

The feature to note in Equations (11) and (12) is that, while there are α and β geometric dependencies in the Cartesian output force, the actuator torques, τ_{m_α} and τ_{m_β}, are decoupled in the x-y plane. The only coupling between the actuators occurs in the z component, as evidenced by Equation (13).

HARDWARE IMPLEMENTATION

Electromechanical Linkage

The manipulandum is depicted as built in Figure 6. The photograph shows the handle shaft, (1), spherical handgrip, (2), and gimbal, (3), components of the mechanism. The gimbal is comprised of three nested pairs of angular contact ball bearings that correspond to the three central revolute pairs j_3, j_4, and j_5 of the 5R linkage depicted in Figure 3. The revolute joints j_1 and j_2 of Figure 3 correspond to the motor shaft ball bearing supports for the manipulandum's two rotary actuators mounted behind the face plates (4) and (6). Together, the combined face and base plate assembly, (4), (6), and (5), form the equivalent of the ground link in Figure 3.

The total length from the center of the handgrip to the center of rotation in the gimbal bearings is 22.9 cm. Given this handle length and the ±25 degree permissible motor shaft angle range, a minimum of ±8.8 cm horizontal handle travel is available, providing a workspace parallel to the x-y plane that is at least 17.6 cm square.

Printed armature permanent magnet DC motors (Model MC23S; Parvex/Alsthom, Spring Valley, NY) were selected for the manipulandum. Because this type of armature is free of iron and has a the large number (153) of commutator bars, the actuators do not exhibit any cogging and have minimal torque ripple (0.5 percent of mean torque level). As a consequence, no evidence of "lumpiness" or "preferred locations" for controlled force output can be detected at the manipulandum handle.

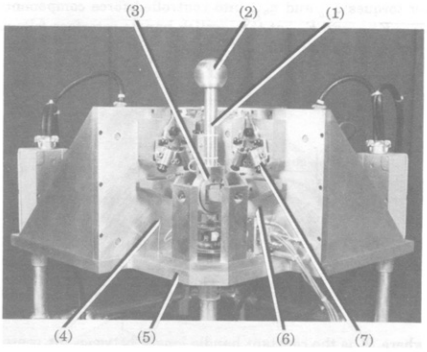

Figure 6. Manipulandum mechanism as built. See text for details.

The motors are driven by PWM transconductance servo amplifiers (Model CX-75; PMI, Commack, NY) that are powered from 115 volt 20 amp single phase service. Since transconductance amplifiers allow direct control of motor current, the dynamic effects of electrical time constants and back EMF can be ignored in the manipulandum. The *continuous* current rating of the amplifiers enables 5 N-m of stall torque to be developed at the actuator shaft. Friction losses, evenly divided between the manipulandum mechanism and the motor bearings and brushes, reduce the available torque at the handle by approximately 0.25 N-m or 5 percent of the continuous rating. This results in approximately 20 N of continuous motor generated force available in each dof at the handgrip.[6] The motor's 3000 RPM rated speed corresponds to translational velocities at the handgrip that are well above both volitional and involuntary human capabilities.

Sensors

Manipulandum displacements are sensed by incremental optical encoders coupled to each motor shaft—*i.e.*, one encoder measures angle α, and the other, β. Each encoders has a 2048 line count per revolution, which upon hardware quadrature decoding yields resolutions of 0.044 degree at the motor shaft and 176 μm at the handgrip. Analog tachometers, integrally mounted on each motor shaft, measure manipulandum velocities $d\alpha/dt$ and $d\beta/dt$ directly .

Uniaxial piezoresistive translational accelerometers (Model EGA-125SR-5D; Entran Devices, Fairfield, NJ) are used to monitor manipulandum accelerations at each motor shaft. By using a cable and pulley arrangement to convert rotation about the horizontal motor shaft into rotation about a vertical axis, each accelerometer only moves in the horizontal plane, thereby eliminating any possibility of a gravity contribution in the rotational acceleration readings. The accelerometers, when combined with externally added thermal drift compensation filters, provide flat frequency response from 0.007 to over 50 Hz.

A two axis strain gauge based "finger-force" miniature joystick (Model 469/20LB; Measurement Systems, Norwalk, CT), combined with a special thrust bearing decoupling mechanism, is embedded in the manipulandum linkage, between the handle shaft and the handgrip. This miniature joystick and decoupler arrangement allows measurement of interface forces tangent to the two dimensional manipulandum workspace, without responding to pure moments applied at the handgrip.

MANIPULANDUM DYNAMIC RESPONSE

The simple lumped parameter model of the manipulandum mechanism, shown in Figure 7, was developed to predict the open loop frequency response of the actuators and linkage to input torques and forces. Because of the approximate decoupling of the α and β axes of the manipulandum, the two axes can be treated independently.

The lumped parameter model is discretized into three inertias separated by two springs. The first spring, with rotational stiffness k_f, represents the flexible shaft coupling that was included between the motor shaft and the gimbal to ease the alignment tolerance requirements for fabrication and assembly of the manipulandum. The second spring, with translational stiffness k_x, is due to the flexible strain gauge beam of the "finger-force" joystick placed between the spherical handgrip and the handle link. The three inertial elements are the rotary inertia of the motor shaft and disk armature, I_r; the gimbal and handle inertia with respect to the shaft axis of rotation, I_g; and the mass of the spherical handgrip, m_s. R_o, is the distance between the center of the handgrip and the gimbal axis of rotation, as defined for Equations (11), (12), and (13).

Quantitative values were assigned to the model elements either by direct measurement or through estimates based on the element dimensions and material properties. The parameter values for Axis 1 (α rotation) and 2 (β rotation) are listed in Table 1. Modal frequencies based on these lumped parameter values were computed for the bond graph structure in Figure 7, subject to the three clamping conditions illustrated in Figure 8. Using the same three clamping conditions, *experimental* frequency and damping coefficients were derived from the response to impulse perturbations as measured by the manipulandum's sensors. All experimental perturbation responses were very lightly damped, with damping ratio $\zeta < 0.10$, allowing the measured damped frequencies in each case to be treated as equal to the natural (*i.e.*, undamped) frequencies.

Model predictions and experimental results for the handle in the "straight-up" position ($\alpha = \beta = 0$) are compared in Table 2. The strong agreement between the model and experiment frequencies for all three clamping conditions demonstrates that the model structure and assigned parameter values are reasonable. The zero Hz frequency under Condition 1 corresponds the free-body mode—*i.e.*, the tendency of the unconstrained manipu-

[6] The amplifiers are capable of 60 N *peak* forces at the handgrip for periods up to 0.5 seconds.

landum handle to fall over when perturbed. Also, both modelled and measured frequencies were not altered significantly (less than 1.0 Hz increase) by handle displacements of up to ±25 degrees from the "straight-up" position.

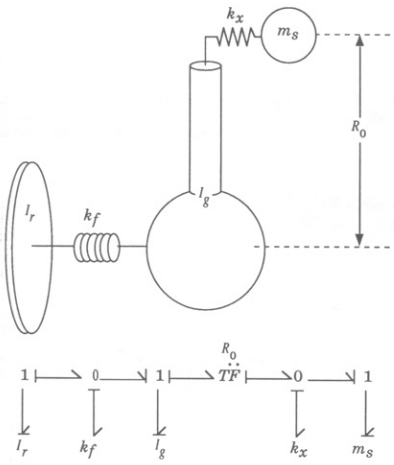

Figure 7. Manipulandum mechanism lumped parameter model.

Axis	I_r* (kg-m^2)	I_g* (kg-m^2)	m_s** (kg)	k_f** (N-m/rad)	k_x** (N/m)	R_o** (m)
1 (α)	0.0028	0.0089	0.125	325	160000	0.229
2 (β)	0.0028	0.0089	0.125	250	160000	0.229

Table 1. Manipulandum lumped model parameters: *estimated value; **measured value.

Most noteworthy of the results in Table 2 is that the frequencies of the first oscillatory mode in the unclamped case (Condition 1), measured at 58 and 48 Hz respectively for Axes 1 and 2, do not change drastically when the rigid clamping of Condition 3 is imposed on the handgrip. This indicates that the grasp of a human hand, with significantly greater compliance at the palm (Reynolds and Falkenberg, 1982) than either the model or experimental clamp, would have even less effect on the manipulandum's first modal frequency. Also of importance is that, at the 12 Hz maximum frequency of human manual output, the structural bandwidth of the manipulandum (dictated by the minimum 48 Hz first mode frequency) contributes only three degrees of phase lag and negligible force magnitude attenuation. Thus, when the manipulandum is programmed to impose controlled mechanical loads on the arm, it is the motor generated simulation that will be felt by the human rather than the negligible contribution of passive mechanical hardware properties.

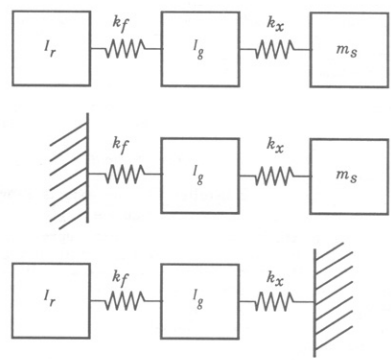

Figure 8. Lumped parameter model and measurement clamping conditions. (*Top*) Condition 1: manipulandum mechanism unclamped. (*Middle*) Condition 2: manipulandum clamped at motor shaft. (*Bottom*) Condition 3: manipulandum clamped at handgrip.

Condition	Axis 1		Axis 2	
	Model (Hz)	Measurement (Hz)	Model (Hz)	Measurement (Hz)
1	0 59 236	0 58 240	0 46 236	0 48 220
2	23 236	22 240	18 236	20 220
3	53 157	54 167	42 156	44 167

Table 2. Lumped parameter model modal frequency predictions versus experimental measurements for three clamping conditions shown in Figure 8.

CONTROL ARCHITECTURE

Load Simulation

Forces at our manipulandum interface can be controlled through two methods. The first is conventional digital control where sampled data from the manipulandum's sensors are processed in real time by control algorithms on a digital computer to produce input commands for the motor servo amplifiers. In principal, any linear or nonlinear, time invariant or time varying controller structure can be implemented by this method, provided that the

computer can carry out the algorithm calculations at the requisite speed.

The second control method relies on a digitally supervised analog control, similar to the approach described by Abul-Haj and Hogan (1987), in which analog signal gains are modulated by multiplying digital to analog converters (MDACs) under digital command from a supervisory computer. The result is a programmable hardwired manipulandum controller capable of producing fundamental mechanical load types with minimal computation.

In this application, the approximate decoupling between the actuator axes permits separate identical joint space feedback circuits around each motor to produce Cartesian endpoint impedances that are decoupled in the x-y plane—*i.e.*, *diagonal* 2×2 stiffness, damping, and inertia matrices. These matrices, however, still contain joint angle dependent terms that, if uncompensated, can affect apparent x-y planar impedance magnitudes by as much as ±20 percent.[7]

The hardwired controller for one axis is represented in block diagram form by Figure 9. $\tau_h(s)$ is the torque input by the human hand, with $\theta(s)$ representing the resultant angular position of the manipulandum handle. I_m is the inertia of the manipulandum handle mechanism summed from the three inertial elements of the lumped parameter model in Figure 7.[8] τ_f is the torque due to internal motor and gimbal mechanism friction. H_m is the voltage-to-torque gain of the transconductance amplifier and motor. $H_p(s)$, $H_v(s)$, $H_a(s)$, and $H_t(s)$, respectively, represent the signal dynamics and gains (including the MDAC modulated gains) associated with the position, velocity, and acceleration sensors at the motor shaft, and the interface torque (*i.e.*, force) as measured by the sensor at the manipulandum handgrip. Because all relevant kinematic variables are measured directly, there is no need to resort to either analog or numerically based differentiation and integration.

$V_d(s)$ is a reference voltage, which may be computer generated, that passes through fixed gain block K_d. By setting all MDAC gains to zero, all analog feedback loops can be cut, leaving $V_d(s)$ to be used for purely digital control signals based on sampled sensor values. Alternatively, it is also possible to combine the digital input with the architecture in Figure 9 to implement a hybrid digital and digitally supervised analog controller.

The block diagram in Figure 9 reduces to the relation

$$\tau_h(s) = \left[\frac{(I_m + I)s^2 + Bs + K}{(1+G)}\right]\theta(s) + \frac{\tau_p}{(1+G)} + \frac{\tau_f}{(1+G)}, \quad (14)$$

with a simulated spring,

$$K = H_p H_m, \quad (15)$$

damper,

$$B = H_v H_m, \quad (16)$$

and inertia element,

$$I = H_a H_m. \quad (17)$$

A dimensionless force feedback gain,

$$G = H_t H_m, \quad (18)$$

can either attenuate or magnify both the simulated impedances and the intrinsic manipulandum inertia and friction. The computer generated reference voltage term,

$$\tau_p(s) = K_d H_m V_d(s) \quad (19)$$

can serve either as a reference torque or a virtual trajectory (Hogan, 1985).

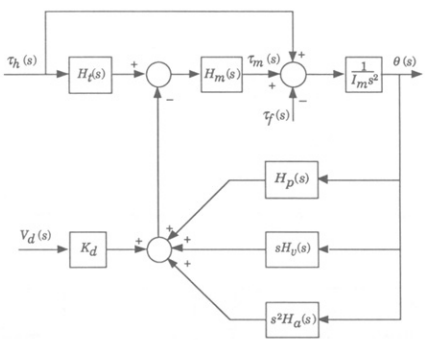

Figure 9. Single axis hardwired digitally-supervised analog impedance controller.

The ability of the manipulandum to simulate both positive and negative (*i.e.*, destabilizing) spring and damper fields, and to augment or mask its inherent inertia and friction according to Equation (14) under digitally supervised analog control has been demonstrated (Adelstein, 1989). In addition, both digital and hybrid control have been employed to generate virtual mechanical objects such as hard "non-sticky" walls and detents (Adelstein, 1989), (Adelstein and Rosen, 1991). Because of directly sensed kinematics and the absence of geometric transformations, update rates exceeding 1 kHz were achievable on a DEC LSI-11/23 computer for both digitally supervised analog and purely digital simulations.

[7] See Adelstein (1989) for details.

[8] I_m can be treated as a single lumped parameter because the 12 Hz operating limit for manual control research is well below the mechanism's first modal frequency listed in in Table 2.

Safety Maintenance

Maintenance of safety for both the human subject and experimental apparatus is a critical issue in the operation of the manipulandum. The human subjects who volunteer to participate in experiments with the apparatus are, in effect, being asked to "shake hands" with a device that has force, velocity, and acceleration capabilities similar to those of an industrial robot. In an industrial setting, however, this type of human interaction is rarely, if ever, tolerated.

Under normal supervised operation, the apparatus poses no hazard to the human subject. Physical contact with any sharp edges or tight corners is prevented by a Delrin cover and leather boot. The cover and the polycarbonate handgrip also insulate the subject from electrical contact with any metal in the device. In addition, all exposed metal surfaces on the manipulandum are well grounded and all electrical inputs properly fused.

The strategy for maintaining safety is simple—make the manipulandum difficult to turn on and extremely easy to turn off. To prevent inadvertent powering of the manipulandum in unsupervised situations, activation of the machine has to follow a deliberate sequence of steps. These steps include: 1) powering the electronic control unit to enable an AC power latching relay; 2) activating the latching relay to power the servo amplifiers; 3) executing computer code which zeros all manipulandum load settings and engages a manual servo amplifier enable switch; and 4) then pressing on the servo amplifier enable switch to allow servo amplifier current to flow through the motors. A failure in any of the system components—electronic control unit, computer, or servo amplifier—prevents completion of the start-up sequence.

The shutdown procedure uses "OR" logic to allow any one of several fault indicators to trigger the immediate removal of input electrical power to all system components other than the computer, the disconnection of the servo amplifiers from the motors, and the short circuiting of the motor terminals. Manipulandum faults that lead to shutdown include: 1) aberrant accelerations due to sudden ballistic movement or high frequency vibration; 2) contact with any of four limit switches—item (7) in Figure 6; and 3) a manual override at any one of several series connected "off" switches. The response actions to these fault conditions are all hardwired; none depend on computer software intervention. The slowest reaction time to cut servo amplifier power to the motors, occurring in response to the first fault condition, is 5 msec. The reaction time is significantly faster for the other two fault conditions. Since power to the system is electromagnetically latched, removal of system electrical power, either because of a manipulandum fault or because of failure in the AC main, requires that the complete start up procedure described above be reinitiated to bring the system back up.

DISCUSSION

This paper has described the design and implementation of a force reflecting manipulandum developed for manual control research. Based on the requirements to study human tremor, a goal of a 12 Hz "effective operating bandwidth" was set, over which the manipulandum is capable of tracking human force and motion with *minimal* phase lag. With performance capable of meeting this goal, the manipulandum brackets the frequency content of volitional human movement, and is therefore able to provide effective kinesthetic coupling to general mechanical simulations.

A number of measures were taken to minimize the manipulandum's intrinsic phase lag—or, equivalently, maximize its bandwidth. The first measure was to design the manipulandum linkage with sufficient structural bandwidth. In this case, a first structural mode at 48 Hz ensures that no more than three degrees of phase lag due to the passive interface's mechanical characteristics will be present over the range of human manual activity . The remainder of the measures affect the amount of computation necessary for real time control, since, by reducing computation, both high update rates and minimal processing latencies can be sustained. By choosing a mechanism configuration that permits joint space control to produce approximately decoupled impedances at the manipulandum endpoint, computer-based geometric transformations are eliminated. Since joint space displacements, velocities, and accelerations are sensed directly, there is no need for computer-based differentiation or integration of kinematic quantities. Furthermore, since the actuators and servo amplifiers selected for the manipulandum produce smooth output torque with negligible intrinsic dynamics, computer-based compensators are unnecessary. Finally, manipulandum safety relies only on hardwired electronics, independent of any computer action.

Together, these computation related measures permitted digital update rates on a DEC LSI-11/23 computer exceeding 1 kHz for simple mechanical object simulations. In addition, by employing a hardwired digitally supervised analog controller, simple mechanical impedance fields, once initiated by the computer, can be implemented without further on-line intervention.

Thus far, the manipulandum has been used for experimental tremor research (Adelstein, 1989), (Chen, 1992). Because of its high bandwidth capabilities, the manipulandum can also serve as a valuable tool in the study of kinesthetic interfaces for virtual environments and teleoperation. Initial plans in this area are to employ the manipulandum for exploring psychophysical effects due to controller update rates and latencies, as well as passive structural bandwidth. These issues related to the temporal characteristics of mechanical environment simulation must be understood to allow the future design of effective kinesthetic interfaces.

ACKNOWLEDGEMENTS

This work was performed in the Evelyn E. and Eric P. Newman Laboratory for Biomechanics and Human Rehabilitation at the Massachusetts Institute of Technology. It was funded in part by grants from NINCDS, Public Health Service, Department of Health and Human Services (5R01-NS17610-03); NIDRR, Department of Education (G008300074); and the Burke Rehabilitation Center, White Plains, NY; and a Fairchild Foundation fellowship.

REFERENCES

Abul-Haj, C.J., and Hogan, N. (1989). An emulation technique for developing improved elbow-prosthesis designs. *IEEE Trans. Biomed. Eng.*, BME-34:724-737.

Adelstein, B.D. (1989). *A Virtual Environment System for the Study of Human Arm Tremor*. Ph.D. dissertation, Dept. of Mech. Eng., M.I.T., Cambridge, MA.

Adelstein, B.D., and Rosen, M.J. (1991). A high performance two degree-of-freedom kinesthetic interface. *Human-Machine Interfaces for Teleoperators and Virtual Environments*, NASA Conference Publication 10071, pp. 108-113.

Albers, J.W., Potvin, A.R., Tourtellotte, W.W., Pew, R.W., and Stribley, R.F. (1973). Quantification of hand tremor in the neurological examination. *IEEE Trans. Biomed. Eng.*, BME-20:27-37.

Asada, H., and Youcef-Toumi, K. (1987). *Direct Drive Robots: Theory and Practice*. MIT Press, Cambridge, MA.

Bejczy, A.K, and Salisbury, J.K. (1980). Kinesthetic coupling between operator and remote manipulator. In *Proceedings of the ASME International Computer Technology Conference*, San Francisco, pp. 97-211.

Carmichael, M.W.J. (1979). Elementary joystick mechanisms. In *Proceedings of the Fifth Congress on Theory of Machines and Mechanisms*, Montréal, pp. 1464-1467.

Chaware, P.R., and Amarnath, C. (1984). A novel wrist joint design for manipulators. In *International Symposium on Design and Synthesis*, Tokyo, pp. 479-482.

Chen, C.-A. (1992). *The Use of Isometric EMG and Force Data to Study the Relationships between Pathological Intention Tremor in Segments of the Upper Extremity*. MS thesis in preparation, Dept. of Mech. Eng., M.I.T., Cambridge, MA.

Desmedt, J.E., ed. (1978). *Physiological Tremor, Pathological Tremors and Clonus, Progress in Clinical Neurophysiology, Vol. 4*, Karger, Basel.

Findley, L.J., and Capildeo, R., eds. (1984). *Movement Disorders: Tremor*, Oxford University Press, New York.

Freund, H.-J., Hefter, H., Homberg, V., and Reiners, K. (1984). Determinants of tremor rate. In Findley, L.J., and Capildeo, R., eds., *Movement Disorders: Tremor*. Oxford University Press, New York, pp. 195-204.

Hogan, N. (1985). Impedance control: An approach to manipulation: Part I—Theory, Part II—Implementation, Part III—Applications. *ASME J. Dyn. Sys. Meas. Control.*, 107:1-24.

Jacobsen, S.C., Smith, F.M., Backman, D.K., and Iversen, E.K. (1991). High performance, high dexterity, force reflective teleoperator II. *Proceedings of the ANS Topical Meeting on Robotics and Remote Systems*, Albuquerque NM.

Jau, B.M. (1991). Anthropometric Remote Manipulator. Technical support package for NASA Tech Brief, Vol. 15, No.4, Item 127.

Lee, R.G., and Stein, R.B. (1981). Resetting tremor by mechanical perturbations: a comparison of essential tremor and parkinsonian tremor. *Ann. Neurol.*, 10:523-531.

Livingstone, S.M., and Crecraft, D.I. (1968). Design of an artificial elbow: an electromechanical solution. In *Basic Problems of Prehension, Movement, and Control of Artificial Limbs*, The Institution of Mechanical Engineers, London, pp. 32-36.

Matthews, P.C.B., and Muir, R.B. (1980). Comparison of electromyogram spectra with force spectra during human elbow tremor. *J. Physiol. (London)*, 302:427-441.

Reynolds, D.D., and Falkenberg, R.J. (1982). Three- and four-degree-of-freedom models of the vibration response of the human hand. In Brammer, A.J., and Taylor, W., eds., *Vibration Effects on the Hand and Arm in Industry*, Wiley, New York, pp. 117-132.

Riley, P.O., and Rosen, M.J. (1987). Evaluating manual control devices for those with tremor disability. *J. Rehabilitation Res. Development*, 24(2):99-110.

Schmidt, E.M. (1973). Electronically controlled load for monkey manipulandum. *Electroenceph. clin. Neurophysiol.*, 35:95-97.

Stiles, R.N., and Randall, J.E. (1967). Mechanical factors in human tremor frequency. *J. appl. Physiol.*, 23:324-330.

Stiles, R.N. (1975). Acceleration time series resulting from repetitive extension-flexion of the hand. *J. appl. Physiol.*, 38:101-107.

Van Cott, H.P., and Kinkade, R.G. (1972). Human Engineering Guide to Equipment Design. U.S. Government Printing Office, Washington DC.